Quantitative analysis of the frictional properties of solid materials at low loads. I. Carbon compounds

Udo D. Schwarz, Oliver Zwörner, Peter Köster, and Roland Wiesendanger
Institute of Applied Physics and Microstructure Research Center, University of Hamburg, Jungiusstrasse 11, D-20355 Hamburg, Germany
(Received 20 February 1997)

Load-dependent studies of the frictional properties of the carbon compounds graphite, diamond, amorphous carbon, and C_{60} were performed by friction force spectroscopy in air and dry argon. During the experiments, the surface was profiled at low loads without wear or plastic deformation. The tips used for profiling were fabricated according to a special production procedure in order to obtain apexes with a well-defined spherical shape and known apex radius. The data obtained were compared with a theoretical model based on the contact mechanical analysis of a Hertzian-type tip/sample contact with small tip radius, low surface energies, but not too low elastic moduli of the tip and sample material. Our experimental results are in excellent agreement with a $F_f \sim F_n^{2/3}$ dependence of the frictional force F_f on the normal force F_n as predicted for this case. These findings suggest that *contact mechanical models*, in spite of being based on continuum elasticity theory, *are valid for tip radii down to a few nanometers* and that the shear stress is constant within the elastic regime. Additionally, it was shown that the friction coefficient $\mu = F_f/F_n$ is not well suited for comparing the tribological behavior of different materials in the case of single-asperity friction. Therefore, an *effective friction coefficient for point-contact-like single-asperity friction* was introduced for the classification of the microscopic frictional properties of materials. As quantitative results, high microscopic friction was found for C_{60} thin films, medium friction for amorphous carbon and diamond, and very low friction for graphite. [S0163-1829(97)00635-8]

I. INTRODUCTION

Frictional forces are familiar from daily life; their understanding is important for the optimization of all kinds of machinery with parts that are in relative motion. Therefore, tribology, the science of friction, wear, and lubrication, has a long history.[1] Nevertheless, the understanding of the fundamental mechanisms of friction on the atomic or molecular level is still poor since most macroscopically measurable frictional effects are dominated by the influence of wear, plastic deformation, lubrication, surface roughness, and surface asperities.

In recent years, however, the field of *nanotribology* was established by introducing new experimental tools, mainly the quartz crystal microbalance,[2–4] the surface force apparatus (SFA),[5–7] and the friction force microscope (FFM),[8–10] which allow the investigation of wearless friction on the nanometer scale. Today, macroscopic friction is believed to be the sum of the frictional effects occurring at many individual small asperities that make the physical contact between the two bodies sliding relative to each other. Thus, the investigation of *point-contact friction*, experimentally realized by a small single-asperity contact of a tip with a suitable sample in the FFM, seems to be especially promising.

The main disadvantage of this technique up to now was the lack of knowledge about the exact nature of the tip/sample contact, contrary to, e.g., the situation in the SFA where the actual tip/sample contact area can be measured independently.[11] For the data presented in this paper, this disadvantage of friction force microscopy/spectroscopy has been overcome by applying specially prepared and characterized tips of exact spherical geometry to sample surface areas which were free of any surface steps. It will be shown that under these conditions, the contact area-load dependence of the tip/sample contact can be described *very accurately* mathematically by contact mechanical methods,[12,13] allowing the extraction of reproducible quantitative data from friction force spectroscopical measurements. Such a mathematical description of the elastic properties of the tip/sample contact is valid *even for tip radii of only a few nanometers although the corresponding contact mechanical treatment is based on continuum elasticity theory*. In this context, a friction coefficient $\tilde{C}$ is introduced that allows a comparison of the frictional properties of two different materials for the case of single-asperity friction without the occurrence of wear.

In order to demonstrate the versatility of this method, we examined the frictional properties of the carbon compounds diamond, graphite, amorphous carbon, and C_{60} thin films. These tribological systems are of great interest from both a fundamental and technological point of view: The samples investigated consist of the same atomic species, but exhibit very different friction, and their specific frictional properties are crucial for many industrial applications (cf. Sec. III). Experiments were performed under ambient conditions as well as in an oxygen-free and water-free argon atmosphere.

II. THEORETICAL BACKGROUND

A. Amontons's law of friction and the multiasperity contact

Already 500 years ago, Leonardo da Vinci recognized that friction is proportional to load and independent from the

(apparent) contact area.[1,14] These facts were later rediscovered by Amontons (1699) who introduced the fundamental friction law

$$F_f = \mu F_l, \tag{1}$$

where the friction coefficient μ is constant for a given material combination in a wide range of externally applied loading forces F_l and independent from the *apparent* contact area. The reason for this behavior, however, remained unclear for a long time.

In order to shed light on the origin of Eq. (1), let us define the mean contact pressure p

$$p = F_l / A \tag{2}$$

and the frictional force per unit area S (the so-called *shear stress*)

$$S = F_f / A. \tag{3}$$

Here, A denotes the *actual* contact area. From its definition, S can generally be a function of the mean contact pressure p, i.e., $S = S(p)$. Nevertheless, it is obvious from Eqs. (2) and (3) that if A is proportional to F_l, p will be constant for all externally applied loading forces F_l. Consequently, $S(p)$ will also be constant for all F_l, resulting in $F_f \sim F_l$.

Greenwood and co-workers showed for the *elastic* regime that the $A \sim F_l$ condition is fulfilled for two bodies with rough surfaces (*multiasperity contact*) if a certain statistical height distribution of the individual surface asperities is assumed.[15–17] Moreover, when the externally applied load F_l increases and the elastic regime is left, *plastic* deformation will increase the area of contact until the mean contact pressure p in both materials (sample and slider) is less than the yield pressure p_y. Thus, since $p \approx p_y = \text{const}$ and $A = F_l / p_y$, i.e., $A \sim F_l$, Amontons's law will be valid for multiasperity contacts in relative motion in both the elastic and the plastic regime.

B. The friction law for a small single-asperity contact of spherical shape

As we saw in the previous section, the reason for the validity of Amontons's law in the case of multiasperity contacts is the proportionality of the actual contact area A to the externally applied loading force F_l. Most single-asperity contacts, however, show a nonlinear contact area-load dependence.[18] This fact allows the investigation of a possible dependence of the shear stress S on the mean contact pressure p. Actually, many examples have already shown that for a *single-asperity contact*, the dependence of friction on load can be strongly nonlinear (see, e.g., Refs. 7,12,13,19–21). It will therefore be the topic of this section to analyze the case of single-asperity friction. For the discussion, the externally applied loading forces are restricted to the elastic regime (the low-load regime[13]), where no wear and no plastic deformation occurs.

For such an experimental approach, it is necessary that the actual contact area A and the frictional force F_f can be determined individually at different loading forces F_l. This is realized in the SFA, as already mentioned in the Introduction, by detecting the actual contact area using the so-called fringes of equal chromatic order technique.[11] In this technique, the visualization of the interference signal is done by means of optical microscopy. Therefore, the contact area cannot be much smaller than $\approx 100\,\mu\text{m}^2$ for an accurate determination of its size, and the effective radii of the crossed mica cylinders which are brought into contact in an SFA experiment are often as large as a few millimeters. Further disadvantages of this method are its limitation to mica or thin films on mica substrates and a lack of spatial resolution.

In this paper, we have chosen an indirect way to determine the contact area A at different loading forces. If the geometry and the elastic properties of tip and sample as well as the externally applied loading forces are known, the contact area in the elastic regime can be calculated using contact mechanical methods.[18] This results in a simple mathematical relationship for a spherical tip on a flat sample. For this scenario, Hertz determined the contact area in the case of absent attractive forces to[22]

$$A = \pi \left(\frac{R F_l}{K} \right)^{2/3}, \tag{4}$$

where R is the radius of the tip and

$$K = \frac{4}{3} \left(\frac{1-\nu_1^2}{E_1} + \frac{1-\nu_2^2}{E_2} \right)^{-1} \tag{5}$$

the effective elastic modulus of the contact (ν_i is Poisson's ratio, E_i is Young's modulus of sphere and flat surface, respectively; $i = 1,2$).

If attractive forces are present, the situation is more complicated.[12,13,23,24] The general mathematical formulation of the problem cannot be solved analytically.[25–27] Nevertheless, depending on where the attractive forces act, analytic approximations can be derived. If attractive forces are only present *inside* the contact area, elastic deformation of tip and sample are described by the Johnson-Kendall-Roberts (JKR) theory.[28] However, if the attractive forces act predominantly *outside* the contact area, the analyses of Bradley[29] and Derjaguin, Muller, and Toporov[30,31] should provide an appropriate description. Decisive for the validity of the different approximations is the numerical value of a nondimensional parameter Φ first introduced by Tabor,[32]

$$\Phi = \left(\frac{9 R \gamma^2}{4 K^2 z_0^3} \right)^{1/3}. \tag{6}$$

Here, γ is the surface energy of tip and sample surface (for equal surfaces) and z_0 the equilibrium distance in contact. When Φ is large ($\Phi > 5$), the JKR model applies, which has been confirmed in many experiments (see, e.g., Refs. 7 and 33). On the other hand, the theories of Bradley[29] and Derjaguin, Muller, and Toporov[30,31] apply for $\Phi < 0.1$. In this case, the influence of attractive forces can be considered as a first approximation by an effective force F_n:

$$F_n = F_l + F_0. \tag{7}$$

F_0 is the sum of the attractive forces between a sphere and a flat surface and can be determined by force-distance curves.[34] Replacing F_l by F_n in Eq. (4) then leads to

$$A=\pi\left(\frac{RF_{\mathrm{n}}}{K}\right)^{2/3}. \tag{8}$$

Detailed mathematical derivations of Eq. (8) for the case of attractive capillary forces can be found in Refs. 13, 35, and 36.

The validity of Eq. (8) has *not yet* been confirmed experimentally since contacts with defined geometry and $\Phi<0.1$ could not be realized up to now; however, evidence for their validity comes from molecular dynamics simulations.[37] Nevertheless, introducing realistic values for the contact of a force microscope tip with an atomically flat sample surface [$R=30$ nm, $\gamma=25$ mJ/m^2 (typical for van der Waals surfaces[38]), $K=50$ GPa, and $z_0=3$ Å], we find a value for Φ of 0.086. Therefore, for force microscope tips with spherical tip apexes in contact with not too soft and atomically flat materials possessing not too high surface energies, the *Hertz-plus-offset model* derived above is expected to provide a good approximation. Under these conditions, we can combine Eq. (8) and Eq. (3), resulting in the following expression for the frictional force:

$$F_{\mathrm{f}}=\pi S\left(\frac{R}{K}\right)^{2/3}F_{\mathrm{n}}^{2/3}=CF_{\mathrm{n}}^{2/3}. \tag{9}$$

It is worth pointing out some consequences of Eq. (9).

(1) As mentioned above, the shear stress S can be a function of the mean contact pressure p. However, it was already recognized in the first friction experiments performed with the SFA that S might just be constant.[5] Recent experimental results with both the SFA (Ref. 7) and the FFM (Refs. 12,13, and 21) gave further evidence for the correctness of this assumption.

(2) If the shear stress S were constant for all mean contact pressures p, F_{f} would be proportional to $F_{\mathrm{n}}^{2/3}$. This gives a significant deviation from the linear law in Eq. (1).

(3) The frictional force in the formula above obviously depends on the radius of the tip, i.e., $F_{\mathrm{f}}\sim R^{2/3}$. In order to obtain an *effective friction coefficient for point-contact-like single-asperity friction* that is independent from such size effects, we will define the new coefficient $\tilde{C}$:

$$F_{\mathrm{f}}=CF_{\mathrm{n}}^{2/3}=\tilde{C}R^{2/3}F_{\mathrm{n}}^{2/3}, \tag{10}$$

which allows a reasonable comparison of measurements obtained with tips exhibiting different apex radii.

(4) Using Eqs. (9) and (10), we find that

$$\tilde{C}=\pi\frac{S}{K^{2/3}}, \tag{11}$$

i.e., $\tilde{C}$ combines the influence of the intrinsic frictional with the elastic properties of a given material combination on the experienced frictional force. However, at this scale, the actual value of the effective elastic modulus K [which is generally determined by Eq. (5)] might significantly be influenced by contamination layers. Hence, it is not possible to derive quantitative exact values for S from $\tilde{C}$ without having an independent measurement of K. For this reason, we will only give numerical values for $\tilde{C}$ in this paper and not for S.

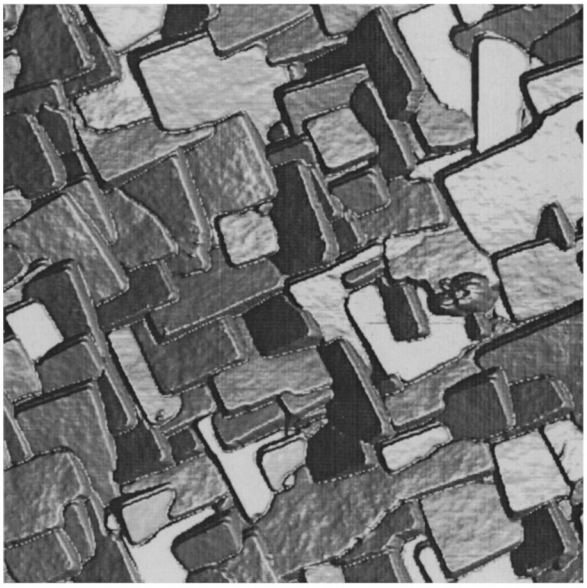

FIG. 1. Force micrograph of the (001)-oriented diamond film investigated in this study (image size: 13 μm$\times$13μm). The largest individual grains exhibit terraces of about 1 μm^2. The tilt of such a terrace against the horizontal image plane is typically 2−5°.

It will be the aim of future work to determine quantitative exact values for K in order to calculate S.

III. EXPERIMENT

A. Samples

1. Diamond

Diamond, known as the hardest material in nature, shows low friction on the macroscopic scale for unlubricated diamond/diamond contacts (friction coefficients down to $\mu=0.05$ were measured) combined with an excellent wear resistance.[39] Moreover, for diamond/diamond contacts lubricated with water, even lower friction coefficients down to ≈ 0.001 were reported.[40] For diamond sliding on metal surfaces, similar results were obtained. For these reasons, the use of diamond cutting tools was established for the machining of hard metals and ceramics. In addition, since diamond has an extremely high melting point and retains its hardness up to very high temperatures, it is very effective as a polishing powder.

Recently, it has become possible to grow polycrystalline diamond films by low-pressure chemical vapor deposition (CVD), enabling the coating of all kind of tools and machinery parts to protect them against wear. Therefore, in order to optimize the tribological properties of diamond coatings, a knowledge of their frictional properties is important.

The polycrystalline diamond film investigated in this study was deposited by the hot-filament CVD technique on an (001)-oriented silicon substrate and shows (001)-oriented facets. The epitaxial orientation of the individual nanocrystals can be confirmed from Fig. 1, displaying a topographical force microscopy image. Image size is 13 μm$\times$13μm. The largest individual grains exhibit terraces of about 1 μm^2. The tilt of such a terrace against the horizontal image plane is typically between 2° and 5°.

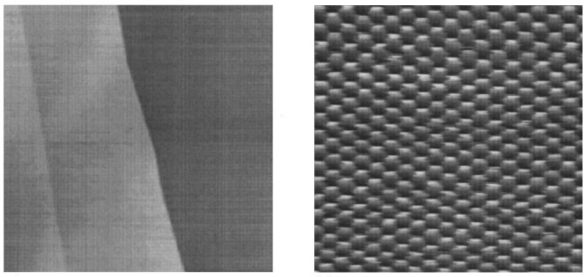

FIG. 2. (a) Large-scale force micrograph of one of the used HOPG samples. Image size was 3 μm$\times$3 μm; steps have the height of one unit cell (3.35 Å) or multiple of this value. The large, atomically flat terraces are well suited for friction force investigations. (b) Atomic-scale force micrograph exhibiting the lattice periodicity (image size: 5 nm$\times$5 nm).

2. Amorphous carbon

Amorphous carbon is widely used as protection layer on magnetic disk media.[41] In order to increase their storage capacity, the distance between disk and slider has to be reduced to a minimum. Therefore, it is important to improve the tribological and mechanical characteristics of the thin film protection layer,[41] and several studies of the frictional properties of such films have already been performed on both unlubricated[42–44] and lubricated[45,46] samples.

The amorphous carbon films used in this study were made by electron-beam evaporation of highly purified graphite (purity better than 99.99%, supplied by Union Carbide) on freshly cleaved muscovite mica. The mica substrate was held at room temperature during evaporation; the background pressure was $\approx 10^{-8}$ Torr, the pressure during evaporation was $\approx 10^{-7}$ Torr. The evaporation rate was 1 Å/s; films with thicknesses in the range of 10–40 nm were grown. Produced in this way, the carbon films exhibited very flat and smooth surfaces in force micrographs. Corrugations of less than 1 nm were typical for areas of several μm^2.

3. Highly oriented pyrolytic graphite

Graphite has been known for a long time to be a material exhibiting low friction ($\mu=0.1$ on the macroscopic scale) even in the absence of any additional lubricant and up to very high temperatures.[39] For this reason, lubricants containing graphite have proved to be very effective under conditions where more conventional lubricants are unsuitable or ineffective.

In their pioneering study, Mate *et al.*[8] reported a friction coefficient of about 0.012 for the atomic-scale friction of a tungsten tip sliding over a freshly cleaved highly oriented pyrolytic graphite (HOPG) surface, which is about an order of magnitude smaller than the macroscopic value mentioned above. This extraordinary low friction coefficient was later confirmed by other scientists (see, e.g., Refs. 34 and 47).

In this study, HOPG with 99.99% purity, supplied by Union Carbide, was used. The samples were freshly cleaved right before the measurements. Figure 2(a) shows a large-scale force micrograph of one of the HOPG samples (image size: 3 μm$\times$3 μm). In Fig. 2(b), an atomic-scale force micrograph (image size: 5 nm$\times$5 nm) exhibits the periodicity of carbon atoms situated at equivalent lattice sites (2.46 Å; see Ref. 48).

4. C_{60} thin films

Soon after the discovery of the C_{60} molecule,[49] there have been speculations about possible unique frictional properties of the material due to the spherical shape of the individual C_{60} molecules and the fact that C_{60} molecules interact only by weak van der Waals interaction, which allows them to rotate freely at room temperature in bulk single crystals[50] as well as in thin films on various types of substrates. The hope was that C_{60} might be some kind of spherical graphite, combining the extraordinary low friction of the graphite surface (see above) with the friction-reducing properties of ball bearings.

However, recent studies of the tribological properties of C_{60} films led to contradictory conclusions.[12,43,51–56] For example, the shear stress between small islands of crystalline C_{60} molecules and an NaCl substrate was found to be extraordinarily low,[56] and low coefficients of friction between a sublimated thin film of C_{60} and a 52100 steel ball[52] or a force microscopy tip[53] down to $\mu=0.06$ were found. On the other hand, other studies report quite high friction between force microscopy tips and C_{60} thin films.[12,43,54]

The C_{60} films used in this study were sublimated in UHV onto *in situ* cleaved single-crystalline GeS(001). Highly purified C_{60} material was filled into the graphite crucible of a Knudsen cell, outgassed at 380 °C for several hours and heated to the evaporation temperature of 420 °C 1 h before the evaporation process was started by opening a shutter. During the evaporation process, the substrate temperature was held at 180 °C; the evaporation rate was 0.07 ML/min and the background pressure 2×10^{-9} Pa. This preparation procedure leads to epitaxial, single-crystalline C_{60} thin films of high quality that show layer-by-layer growth. Due to the crystallinity and the epitaxy of the growing C_{60} islands, a sharp low-energy electron diffraction pattern is obtained.

A force micrograph of the sample used for the friction force spectroscopical measurements presented in this study is displayed in Fig. 3 (image size: 2 μm$\times$2 μm); molecularly smooth terraces of some 100 nm^2 are visible. Nominal coverage was $\approx$2 ML. More details regarding the preparation procedure and the growth modes of C_{60} thin films on GeS substrates can be found in Ref. 57.

B. Preparation of tips with well-defined spherical apexes

We have seen in Sec. II B that for the validity of Eq. (9), it is necessary to have a well-defined tip/sample contact where a tip possessing an exactly spherical apex even on the nanometer scale profiles a flat area of the sample surface. Actually, many experiments performed in our laboratory have shown that the exact shape of the tip end is very critical (see Sec. V). Moreover, tip radii should be small, i.e., they should not exceed about 100 nm.

This was realized by the contamination of doped single-crystalline silicon tips[58] with amorphous carbon in a transmission electron microscope. The tips, having typical radii of 5–15 nm without contamination, were coated with a layer of amorphous carbon of variable thickness using electron-beam deposition. Molecules from the residual gas were ionized in

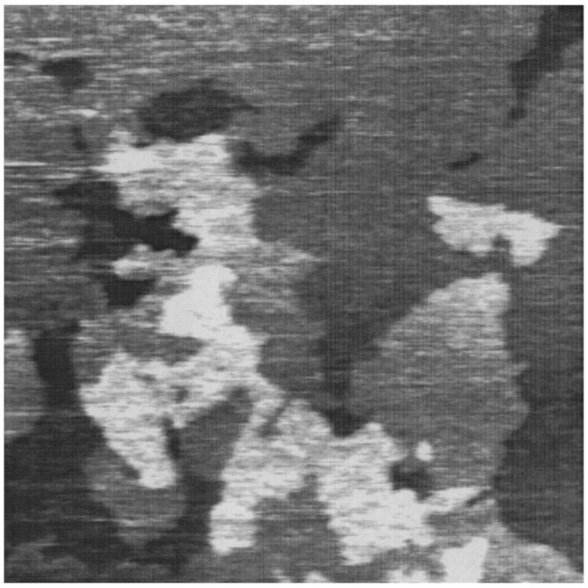

FIG. 3. Force micrograph of the C_{60} thin film sample (image size: 2 μm$\times$2μm). Molecularly smooth terraces of some 100 nm^2 are visible; the step height between individual terraces is 1 ML ($\approx$ 1 nm). Nominal coverage of the sample was $\approx$ 2 ML.

the electron beam and accelerated towards the tip end. There, the molecules spread out evenly due to their charge, forming a well-defined spherical tip apex.

The exact composition of the contamination layer is unknown and depends on the composition of the residual gas in the electron microscope. However, an analysis by means of energy dispersive x-ray emission (EDX) revealed that the ratio of the relative intensities of the silicon and the oxygen peak (the oxygen peak arises from the native silicon oxide at the surface of the silicon tip) was nearly unchanged during the deposition, whereas the carbon peak was continuously growing. Further atomic species except copper (from the holder) and silver (from the silver paint used for connection) could not be identified. Therefore, the tip apexes consist presumably of amorphous carbon, hydrogen (which cannot be detected by EDX), and traces of oxygen, as it is usually assumed for electron-beam-deposited material.[59,60] Tip radii ranging from 5 nm up to more than 100 nm could be produced by varying the deposition time from some minutes up to more than an hour. Three examples of tips prepared using this method are shown in Fig. 4. A more detailed description of the tip preparation procedure will be published elsewhere.[61]

FIG. 4. Transmission electron micrographs of three different tips with spherical apexes prepared according to the procedure described in the text. The apex of the tip presented in (a) has a radius of (21$\pm$5) nm, the radius of the tip end displayed in (b) is (35 $\pm$5) nm, and the tip shown in (c) has an apex radius of (112$\pm$5) nm.

C. Force measurements

The scanning and friction force microscopy/spectroscopy investigation was carried out at room temperature with a commercially available instrument.[62] Normal and lateral forces were measured simultaneously,[9,10] and care was taken that no steps were visible in the topography during the acquisition of the spectroscopical friction data in order to avoid a crosstalk between topography and friction signal. The normal forces F_n and the adhesion F_0 [cf. Eq. (7)] were determined by force-distance curves. F_n was set to be zero at the point where the cantilever left the surface.

All spectroscopical measurements were performed with a sliding speed of 2.78 μm/s; sliding distance was 1 μm. Along such a line, the acting frictional force was measured 512 times in forward as well as in backward scan direction with equal time between individual measurements. The average of these 512 individual measurements represents one data point in the $F_f(F_n)$ plots of the result part. For each normal force, five scan lines were recorded.

For all measurements, rectangular single-crystalline silicon cantilevers[58] were used whose dimensions were accurately determined by means of electron microscopy. From these dimensions, spring constants in z direction ($c_z=F_n/z$) in the range from 0.014 N/m to 0.49 N/m and for torsion ($c_{tor}=F_f/\beta$;β is the torsional angle) from 20 μN/rad to 420 μN/rad were calculated. Tip radii were varied from 5 nm to about 100 nm (see Sec. III B).

Since it is known that humidity might significantly influence the frictional behavior,[63–65] measurements were performed both under ambient conditions and in a water-free and oxygen-free argon atmosphere. In air, the relative humidity was 40$-$60 %. The argon chamber[66] was specially designed for scanning probe applications. The content of water in all measurements was below 1 ppm; the oxygen content might occasionally be increased from below 1 ppm to some ppm due to an interrupted gas flow during measurements, which was shut off in order to obtain the most stable conditions. All measurements were carried out at room temperature.

D. Data analysis

For data analysis, S was assumed to be constant. Additionally, a small offset $F_{off}(|F_{off}| \ll |F_0|)$ of the fitted curves to negative loads had to be introduced in order to account for an uncertainty in the correct determination of F_0.[34] Equation (9) then changes to

$$F_f = \tilde{C} R^{2/3} (F_n - F_{off})^{2/3}. \tag{12}$$

In order to ensure a correct treatment of the statistical and systematical errors of the individual data sets, Eq. (12) was not directly fitted, but the procedure was applied that is described in detail in Ref. 34. The calculation of the mean values for $\tilde{C}$ over all measurements of a certain material combination was done as follows. First, the $\tilde{C}$ obtained with the same cantilever were averaged. The total average of *all*

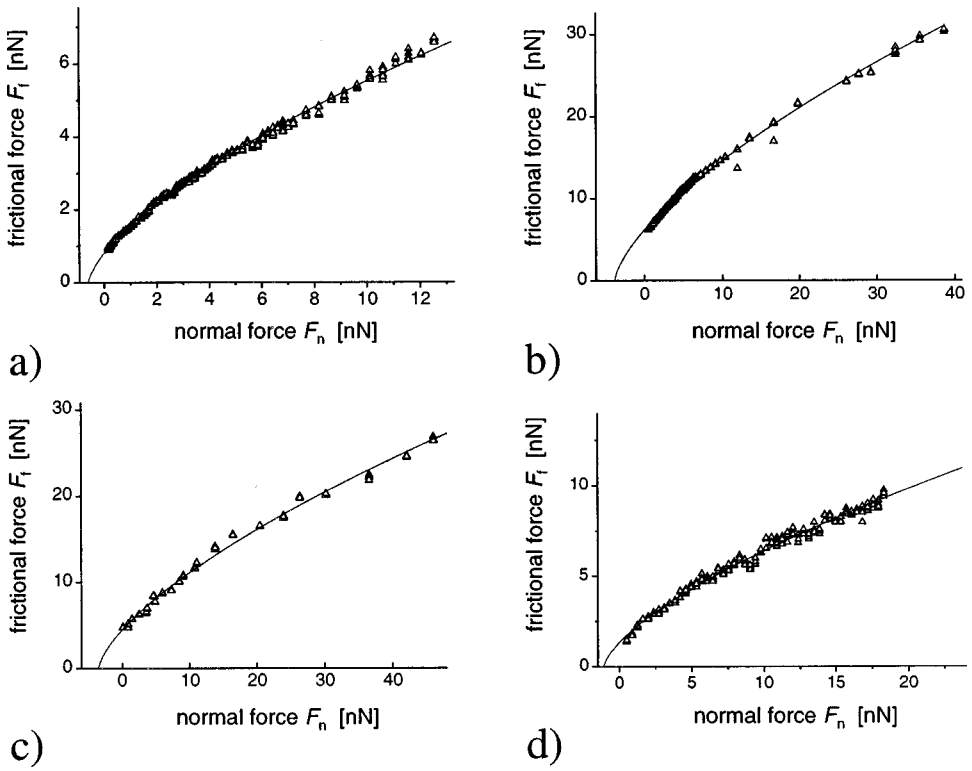

FIG. 5. The frictional force F_f as a function of the normal force F_n, measured on amorphous carbon with well-defined spherical tips in argon atmosphere (content of H_2O below 1 ppm). All curves show excellent agreement with theoretical fits according to Eq. (12). The data presented in (a) were obtained using a tip with an apex radius of $R=(17\pm5)$nm; $n=395$ individual data points are displayed. The adhesion F_0 was 4.6 nN, $\tilde{C}$ and F_{off} were calculated to $\tilde{C}=(0.17\pm0.09)$ $nN^{1/3}nm^{-2/3}$ and $F_{off}=-0.4$ nN. For (b), the relevant parameters were $R=(58\pm7)$ nm, $n=288$, $F_0=25$ nN, $\tilde{C}=(0.17\pm0.07)$ $nN^{1/3}nm^{-2/3}$, $F_{off}=-3.9$ nN; for (c), $R=(58\pm7)$ nm, $n=125$, $F_0=32.6$ nN, $\tilde{C}=(0.13\pm0.05)$ $nN^{1/3}nm^{-2/3}$, $F_{off}=-3.5$ nN; and for (d), $R=(7\pm2)$ nm, $n=245$, $F_0=10.6$ nN, $\tilde{C}=(0.35\pm0.15)$ $nN^{1/3}nm^{-2/3}$, $F_{off}=-1.1$ nN.

measurements was then extracted by averaging the $\tilde{C}$ of the different cantilevers. This stepwise procedure is necessary to calculate reasonable errors for $\tilde{C}$; otherwise, systematical errors arising from cantilever dimensions might be overestimated or underestimated.

IV. RESULTS

A. Friction force spectroscopy of carbon compounds performed in argon atmosphere

Figure 5(a) shows results of a measurement carried out in argon atmosphere on amorphous carbon using a spherical tip with a radius of (17 ± 5) nm prepared as described in Sec. III B. 395 individual line scans were analyzed; F_0 was determined to 4.6 nN. The fit according to Eq. (12) resulted in excellent agreement between experimentally obtained data and theory; values of $\tilde{C}=(0.17\pm0.09)nN^{1/3}nm^{-2/3}$ and $F_{off}=-0.4$ nN were calculated. Comparing F_{off} to F_0, we find that the condition $|F_{off}|\ll|F_0|$ introduced above is fulfilled.

The results presented in Figs. 5(b) were also obtained on amorphous carbon in argon atmosphere, but with a tip exhibiting an apex radius of (58 ± 10) nm. Here, 288 individual line scans were analyzed, predominantly at very low forces where the deviation from the linear behavior is most prominent. The adhesion was, due to the larger tip radius, 25 nN; an offset force of $F_{off}=-3.9$ nN was determined by the fit. Much higher friction was measured compared with Fig. 5(a); the frictional force at $F_n=10$ nN, e.g., is about three times larger (≈15 nN) than the frictional force of only 5.5 nN observed in Fig. 5(a). *Therefore, applying a classical analysis in terms of the friction coefficient μ, a value of μ three times higher would be derived for the second sample compared with the first sample, even though the same sample and identical tip material were used.* However, the calculated numerical value of $\tilde{C}=(0.17\pm0.07)nN^{1/3}nm^{-2/3}$ for this second measurement is in excellent agreement with the value of $\tilde{C}$ obtained in the first measurement as well as with the mean value $\tilde{C}^{a\text{-}C}_{argon}=(0.158\pm0.022)nN^{1/3}nm^{-2/3}$ obtained by averaging four measurements that were performed with a total of three different tips (cf. Table I).

These results already demonstrate that consideration of the geometry of the tip/sample contact is mandatory if meaningful comparisons of the frictional properties between different measurements and different materials should be made. If, however, the geometry is considered, good reproducibility of the measured data is obtained. The $F_f(F_n)$ curve displayed in Fig. 5(c) was acquired with identical tip and sample about 2 h after the data shown in Fig. 5(b), leading to $\tilde{C}=(0.13\pm0.05)nN^{1/3}nm^{-2/3}$. Even in the measurement presented in Fig. 5(d) for which the measured

TABLE I. Relevant data for the measurements performed on amorphous carbon in argon atmosphere. Averaging the first four values for $\widetilde{C}$ yields a mean value $\widetilde{C}^{a\text{-C}}_{\text{argon}} = 0.158 \pm 0.022 \text{nN}^{1/3}\,\text{nm}^{-2/3}$.

Measurement no.	1	2	3	4	5
Tip no.	1	1	2	3	4
Tip radius (nm)	58 ± 10	58 ± 10	24 ± 5	17 ± 5	7 ± 2
c_z (N/m)	0.078 ± 0.015	0.078 ± 0.015	0.025 ± 0.005	0.014 ± 0.003	0.21 ± 0.04
c_{tor} (μN/rad)	130 ± 17	130 ± 17	36 ± 5	20 ± 3	310 ± 40
No. of data points	288	125	185	395	245
Adhesion F_0 (nN)	25	32.6	6.1	4.6	10.6
$\widetilde{C}$ ($\text{nN}^{1/3}\,\text{nm}^{-2/3}$)	0.17 ± 0.07	0.13 ± 0.05	0.15 ± 0.08	0.17 ± 0.09	0.35 ± 0.15
Offset force F_{off} (nN)	-3.9	-6.6	-1.3	-0.4	-1.1

$\widetilde{C} = (0.35 \pm 0.15)\text{nN}^{1/3}\,\text{nm}^{-2/3}$ was by far the most significant deviation from $\widetilde{C}^{a\text{-C}}_{\text{argon}}$, the mean value is only slightly outside the error range.

However, the adhesion of the data displayed in Fig. 5(d) was unusually high ($F_0 = 10.6$ nN) for a tip with such a small tip radius [$R = (7 \pm 2)$ nm], suggesting a contamination of the tip/sample contact by adsorbates. Such a contamination could probably explain at least part of the observed increment of $\widetilde{C}$. Usually, tip and sample were inserted in the argon chamber from air without further sample preparation; only graphite was cleaved *in situ* before measurement. Therefore, contaminants that do not desorb in the water-free argon atmosphere (hydrocarbon compounds, for example) influence the tribological properties of the tip/sample contact by both modifying the local shear stress S as well as the effective value of K of the tip/sample contact. Nevertheless, friction studies performed in ambient air (see Sec. IV B) are reasonable because they represent realistic conditions, and comparative studies in argon atmosphere help evaluating the influence of the water film on the observed friction.

Figure 6 shows $F_f(F_n)$ plots of the other investigated carbon compounds diamond [Fig. 6(a)], C_{60} [Fig. 6(b)], and HOPG [Fig. 6(c)]. The data for diamond and C_{60} are again in excellent agreement with the theoretical model of Eq. (12). For diamond, a value of $\widetilde{C}$ of $(0.21 \pm 0.11)\text{nN}^{1/3}\,\text{nm}^{-2/3}$ was determined which is very close to the average of $C^{\text{dia}}_{\text{argon}} = (0.158 \pm 0.061)\text{nN}^{1/3}\,\text{nm}^{-2/3}$ (cf. Table II), and for C_{60}, $\widetilde{C} = (0.82 \pm 0.33)\text{nN}^{1/3}\,\text{nm}^{-2/3}$ was calculated. In the latter case, however, a comparison with the average value over all C_{60} measurements $\widetilde{C}^{C_{60}}_{\text{argon}} = (0.67 \pm 0.22)\text{nN}^{1/3}\,\text{nm}^{-2/3}$ is problematic, since due to the small terraces on the C_{60} sample, only two measurements could be successfully completed.

On HOPG [Fig. 6(c)], we observed a frictional force that is near the noise level of our FFM, causing large fluctuations of the data points. Calculation of $\widetilde{C}$ resulted in very low values [$\widetilde{C} = (0.0018 \pm 0.0008)\text{nN}^{1/3}\,\text{nm}^{-2/3}$ for the measurement presented in Fig. 6(c) or $\widetilde{C} = (0.0012 \pm 0.0009)\text{nN}^{1/3}\,\text{nm}^{-2/3}$ on average]. However, due to the

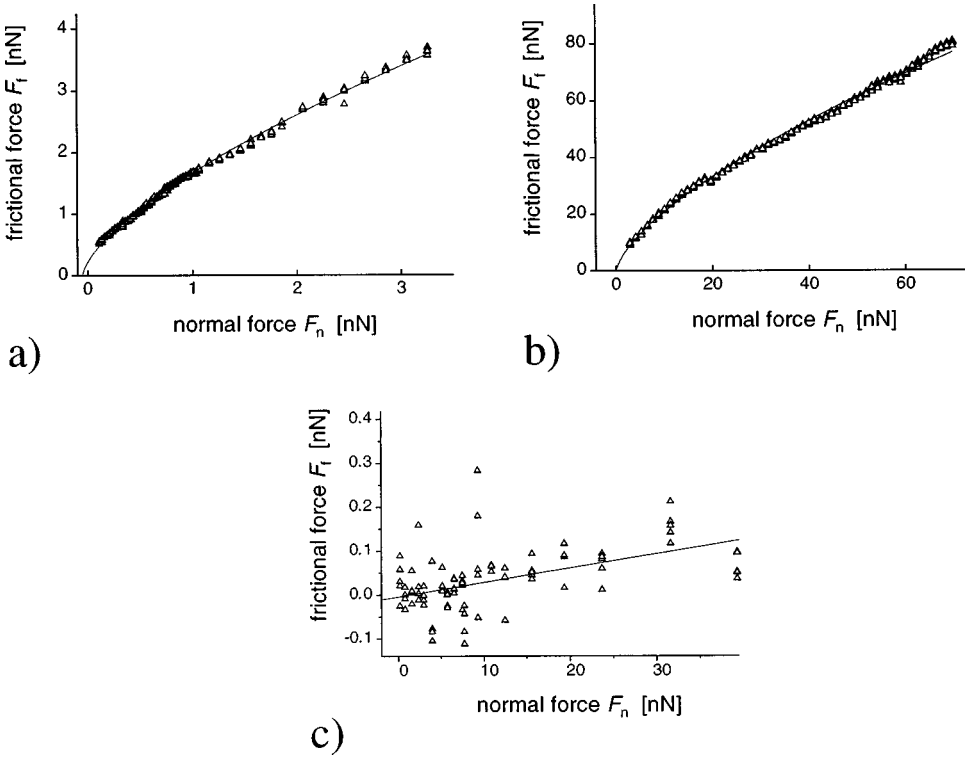

FIG. 6. $F_f(F_n)$ plots for different carbon compounds performed in argon atmosphere. (a) Diamond, $R = (24 \pm 5)$ nm, $n = 355$, $F_0 = 3.6$ nN, $\widetilde{C} = (0.21 \pm 0.11)$ $\text{nN}^{1/3}\,\text{nm}^{-2/3}$, $F_{\text{off}} = -0.05$ nN. (b) C_{60} thin film, $R = (13 \pm 2)$ nm, $n = 205$, $F_0 = 4.1$ nN, $\widetilde{C} = (0.82 \pm 0.33)$ $\text{nN}^{1/3}\,\text{nm}^{-2/3}$, $F_{\text{off}} = 0$ nN. (c) HOPG, $R = (26 \pm 5)$ nm, $n = 65$, $F_0 = 5.3$ nN, $\widetilde{C} = (0.0018 \pm 0.0008)\text{nN}^{1/3}\,\text{nm}^{-2/3}$, $F_{\text{off}} = 2.9$ nN. Additionally, for comparison, a classical friction coefficient $\mu = 0.008 \pm 0.005$ was calculated for HOPG.

TABLE II. Mean values of $\tilde{C}$ for the materials investigated.

Material	Atmosphere	No. of measurements	No. of tips used	Mean value of $\tilde{C}$ ($nN^{1/3}nm^{-2/3}$)
Amorphous carbon	argon	4	3	0.158 ± 0.022
Amorphous carbon	air	6	2	0.450 ± 0.042
Diamond	argon	8	5	0.158 ± 0.061
Diamond	air	6	5	0.263 ± 0.060
C_{60}	argon	2	2	0.67 ± 0.22
HOPG	argon	2	2	0.0012 ± 0.0009

high influence of noise, a comparison of obtained data with the theory of Sec. II B is not very fruitful. Nevertheless, in order to give an impression of the low friction on HOPG, we additionally applied a classical analysis in terms of the friction coefficient μ according to Eq. (1) (but again allowing an offset force) that resulted in $\mu = 0.008 \pm 0.005$. Generally, we can say that the friction on HOPG in argon atmosphere is nearly vanishing and the classical friction coefficient is well below $\mu = 0.02$.

B. Friction force spectroscopy of carbon compounds performed under ambient conditions

Figure 7 shows $F_f(F_n)$ plots of amorphous carbon [Figs. 7(a) and 7(b)], diamond [Fig. 7(c)] and HOPG [Fig. 7(d)], but the plots now display data that were acquired in air. Qualitatively, the results are identical with the situation in argon. For amorphous carbon and diamond, comparatively high friction and good agreement of measured data with the fit curves is observed, whereas for HOPG friction is again nearly vanishing. The comparison of the two measurements carried out on amorphous carbon demonstrates that a knowledge of the exact structure of the tip/sample contact under ambient conditions is as important as it is for measurements performed in argon: In spite of observing a friction three times higher in Fig. 7(b) than in Fig. 7(a), identical numerical values were calculated for $\tilde{C}$ (see figure caption). The results of the averaging are given in Table II for amorphous carbon and diamond. C_{60} thin film samples were not investigated in air since they are known to be unstable under ambient conditions.[57]

V. DISCUSSION

It has been surprising[67] up to now why the response of the friction to a change in load had not resulted in a 2/3 power law as one might expect from the contact mechanical theory reviewed in Sec. II B, but power laws from 1/2 (Ref. 64) to linear (Ref. 67) have been found. Due to the diversity of experimental data obtained, it has been unclear which contact mechanical model would be suitable for the description of the tip/sample contact in force microscopy. In some cases, the JKR model[65] or a modified JKR model[21] have been applied successfully. Moreover, since a model generally applicable to all data could not be derived, there were also speculations about the limits of contact mechanical models, which

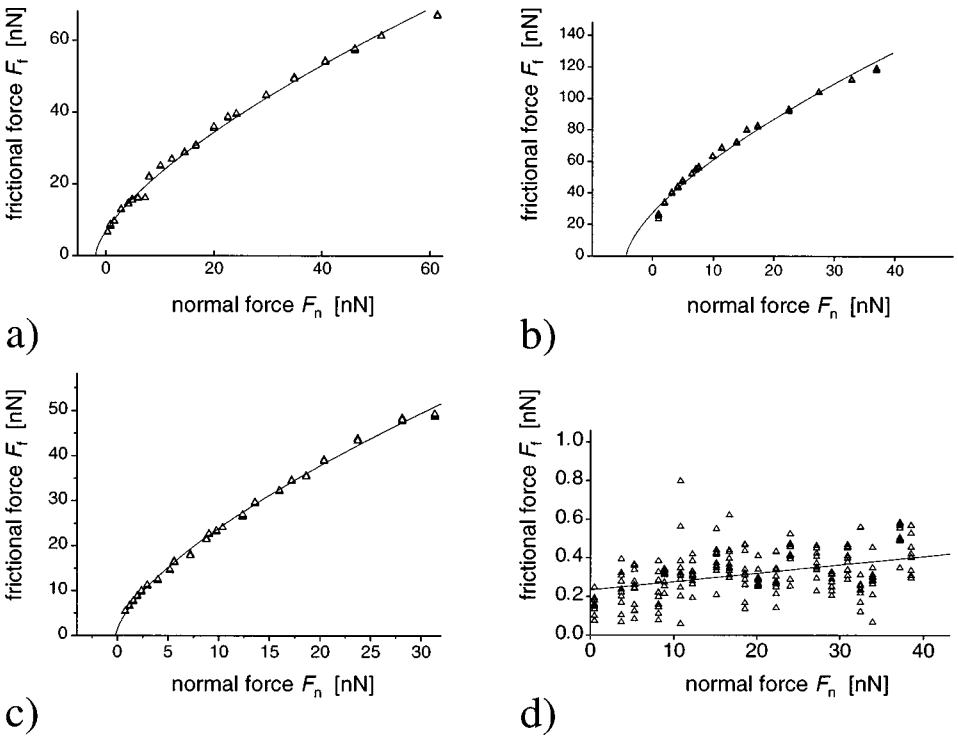

FIG. 7. $F_f(F_n)$ plots for different carbon compounds performed under ambient conditions. (a) Amorphous carbon, $R = (20 \pm 5)$ nm, $n = 110$, $F_0 = 39$ nN, $\tilde{C} = (0.51 \pm 0.23)$ $nN^{1/3}nm^{-2/3}$, $F_{off} = -1.4$ nN. (b) Amorphous carbon, $R = (92 \pm 8)$ nm, $n = 90$, $F_0 = 156$ nN, $\tilde{C} = (0.51 \pm 0.22)$ $nN^{1/3}nm^{-2/3}$, $F_{off} = -4.3$ nN. (c) Diamond, $R = (75 \pm 15)$ nm, $n = 120$, $F_0 = 23.0$ nN, $\tilde{C} = (0.29 \pm 0.13)$ $nN^{1/3}nm^{-2/3}$, $F_{off} = -0.2$ nN. (d) HOPG, $R = (20 \pm 5)$ nm, $n = 199$, $F_0 = 13.0$ nN, $\mu = 0.005 \pm 0.003$. For (a), (b), and (c), the observed $F_f(F_n)$ behavior is in excellent agreement with the predicted $F_f \sim F_n^{2/3}$ dependence.

are all based on continuum elasticity models, in the case of very small tip radii.

Nevertheless, the data presented above shows that the friction model leading to Eq. (12) may be applied to most of the samples investigated with good agreement. From the experiments, we can therefore confirm the *excellent validity of the Hertz-plus-offset model for the description of the dependence of the contact area on the normal force for a sphere/flat contact* in the Bradley regime ($\Phi < 0.1$). Simultaneously, the *validity of contact mechanical theories down to tip radii of only a few nanometers* is confirmed.

However, we would like to point out that the observed behavior of friction on load depended critically on the shape of the tip in all cases. Using tips as provided by the manufacturers resulted in force laws of $F_f \sim (F_n)^m$ with $0.4 < m < 1.2$ at low loads due to the undefined tip/sample contact. Results were in good agreement with the $F_f \sim F_n^{2/3}$ law only if tips were used which were produced according to the preparation procedure described in Sec. III B. Consequently, the interpretation of force microscopical/spectroscopical results in terms of a sphere/flat contact cannot be more than a very crude approximation if tips are used whose shape on the nanometer scale is only approximately (and not *exactly*) spherical. However, even for the specially prepared tips, deviations from the 2/3 power law were observed if the tip apex showed the smallest deviation from the spherical shape (e.g., due to wear). Therefore, in order to prevent wear, the applied normal forces have to be low, and the shape of the tip has to be checked repetitively and routinely after a certain number of experiments. In our case, we determined the exact shape of every tip not only by transmission electron microscopy, but also by imaging a special test sample before and after each individual measurement series.[61]

Another result from our measurements was that *friction is directly proportional to the contact area* in the applied pressure range. That means that the shear stress S is constant, as it was already expected (see Sec. II B). Using this result, we could derive that $C_{\text{argon}}^{\text{C}_{60}} > C_{\text{argon}}^{a\text{-C}} \approx C_{\text{argon}}^{\text{dia}} \gg C_{\text{argon}}^{\text{HOPG}}$ for measurements in argon atmosphere, and $C_{\text{air}}^{a\text{-C}} > C_{\text{air}}^{\text{dia}} \gg C_{\text{air}}^{\text{HOPG}}$ for measurements under ambient conditions. As far as comparative measurements in air and in argon atmosphere were successful, it was found that (if the friction was not already extremely low in air as in the case of HOPG) the friction decreased significantly in a water−free argon atmosphere. Numerically, we derived a ratio $C_{\text{air}}^{a\text{-C}}/C_{\text{argon}}^{a\text{-C}}$ of $1.66^{+1.66}_{-0.73}$ and a ratio $C_{\text{air}}^{\text{dia}}/C_{\text{argon}}^{\text{dia}}$ of $2.36^{+1.50}_{-0.97}$.

VI. CONCLUSION

To summarize, we presented load-dependent measurements of the frictional force obtained on different carbon compounds. Specially prepared well-defined single-asperity tips were used for the experiments performed in argon atmosphere as well as under ambient conditions at low loads (i.e., without the occurrence of wear or plastic deformation). The data can be explained using a theoretical model based on a Hertzian-type tip/sample contact. Within this theory, it was shown that the ''Hertz-plus-offset'' model which predicts a $A \sim F_n^{2/3}$ dependence of the contact area on the normal force works well for a tip/sample contact in the Bradley regime (Tabor's parameter $\Phi < 0.1$). Using these results, it was additionally shown that friction is proportional to the contact area and that the shear stress was constant within the applied pressure range, leading to a $F_f \sim F_n^{2/3}$ dependence of the measured frictional forces F_f on the normal forces F_n. Moreover, it could be demonstrated that the classical friction coefficient μ is not well suited for a comparison of the frictional behavior of materials in the case of single-asperity friction, and an effective friction coefficient for point-contact-like single-asperity friction $\tilde{C}$ was introduced for the classification of the nanoscopic frictional properties of materials. High friction was found for C_{60} thin films, medium friction for amorphous carbon and diamond, and nearly vanishing friction for graphite.

ACKNOWLEDGMENTS

We are indebted to W. Allers, H. Bluhm, H. Hölscher, A. Schwarz, and K. L. Johnson for helpful discussions. Additionally, we would like to thank R. Anton, D. Lauter, and I. Schneidereit for help with the transmission electron microscope and for the EDX analysis, K. Schiffmann for the diamond sample, W. Pfützner for the amorphous carbon films, and L. Yu for the C_{60} films. Financial support from the Deutsche Forschungsgemeinschaft (Grant No. WI 1277/2-2) is gratefully acknowledged.

[1] D. Dowson, *History of Tribology* (Longman, London, 1979).
[2] J. Krim and A. Widom, Phys. Rev. B **38**, 12 184 (1988).
[3] E. T. Watts, J. Krim, and A. Widom, Phys. Rev. B **41**, 3466 (1990).
[4] J. Krim, E. T. Watts, and J. Digel, J. Vac. Sci. Technol. A **8**, 3417 (1990).
[5] J. N. Israelachvili and D. Tabor, Wear **24**, 386 (1973).
[6] B. J. Briscoe and D. C. B. Evans, Proc. R. Soc. London, Ser. A **380**, 389 (1982).
[7] A. M. Homola, J. N. Israelachvili, P. M. McGuiggan, and M. L. Gee, Wear **136**, 65 (1990).
[8] C. M. Mate, G. M. McClelland, R. Erlandsson, and S. Chiang, Phys. Rev. Lett. **59**, 1942 (1987).
[9] O. Marti, J. Colchero, and J. Mlynek, Nanotechnology **1**, 141 (1990).
[10] G. Meyer and N. M. Amer, Appl. Phys. Lett. **57**, 2089 (1990).
[11] J. N. Israelachvili, J. Colloid Interface Sci. **44**, 259 (1973).
[12] U. D. Schwarz, W. Allers, G. Gensterblum, and R. Wiesendanger, Phys. Rev. B **52**, 14 976 (1995).
[13] U. D. Schwarz, H. Bluhm, H. Hölscher, W. Allers, and R. Wiesendanger, in *The Physics of Sliding Friction*, Vol. 311 of *NATO Advanced Study Institute, Series E: Applied Sciences*, edited by B. N. J. Persson and E. Tossati (Kluwer Academic Publishers, Dordrecht, 1996), pp. 369−402.
[14] F. P. Bowden and D. Tabor, *The Friction and Lubrication of Solids* (Clarendon Press, Oxford, 1950).

[15] J. A. Greenwood and J. B. P. Williamson, Proc. R. Soc. London, Ser. A **295**, 300 (1966).
[16] J. A. Greenwood and J. H. Tripp, Trans. ASME Ser. E, J. Appl. Mech. **34**, 153 (1967).
[17] J. A. Greenwood, Trans. ASME Ser. F, J. Lubrication Technol. **89**, 81 (1967).
[18] For a good review on contact mechanical models, see K. L. Johnson, *Contact Mechanics* (Cambridge University Press, Cambridge, 1985).
[19] C. A. J. Putman, M. Igarashi, and R. Kaneko, Appl. Phys. Lett. **66**, 3221 (1995).
[20] E. Meyer, R. Lüthi, L. Howald, M. Bammerlin, M. Guggisberg, and H.−J. Güntherodt, J. Vac. Sci. Technol. B **14**, 1285 (1996).
[21] R. W. Carpick, N. Agrait, D. F. Ogletree, and M. Salmeron, J. Vac. Sci. Technol. B **14**, 1289 (1996).
[22] H. Hertz, J. Reine Angew. Math. **92**, 156 (1881).
[23] K. L. Johnson, Proc. R. Soc. London, Ser. A **453**, 163 (1997).
[24] K. L. Johnson, in *Micro/Nanotribology and Its Applications*, Vol. 330 of *NATO Advanced Study Institute, Series E: Applied Science*, edited by B. Bhushan (Kluwer Academic Publishers, Dordrecht, 1997), pp. 151−168.
[25] A. Burgess, B. D. Hughes, and L. R. White (unpublished).
[26] D. Maugis, J. Adhesion Sci. Technol. **1**, 105 (1987).
[27] D. Maugis, J. Colloid Interface Sci. **73**, 294 (1992).
[28] K. L. Johnson, K. Kendall, and A. D. Roberts, Proc. R. Soc. London, Ser. A **324**, 301 (1971).
[29] R. S. Bradley, Philos. Mag. Suppl. **13**, 853 (1932).
[30] B. V. Derjaguin, V. M. Muller, and Y. P. Toporov, J. Colloid Interface Sci. **53**, 314 (1975).
[31] V. M. Muller, V. S. Yuschenko, and B. V. Derjaguin, J. Colloid Interface Sci. **92**, 92 (1983).
[32] D. Tabor, J. Colloid Interface Sci. **58**, 2 (1977).
[33] J. N. Israelachvili, E. Perez, and R. K. Tandon, J. Colloid Interface Sci. **78**, 260 (1980).
[34] U. D. Schwarz, P. Köster, and R. Wiesendanger, Rev. Sci. Instrum. **67**, 2560 (1996).
[35] A. Fogden and L. R. White, J. Colloid Interface Sci. **138**, 414 (1990).
[36] D. Maugis and B. Gauthier-Manuel, J. Adhesion Sci. Technol. **8**, 1311 (1994).
[37] J. Belak and I. F. Stowers, in *Fundamentals of Friction: Microscopic and Macroscopic Processes*, edited by I. L. Singer and H. M. Pollock (Kluwer Academic Publishers, Dordrecht, 1992), pp. 511−520.
[38] J. N. Israelachvili, *Intermolecular and Surface Forces* (Academic Press, London, 1991).
[39] F. P. Bowden and D. Tabor, *The Friction and Lubrication of Solids* (Ref. 14), pp. 158−164.
[40] Y. Tzeng, Appl. Phys. Lett. **63**, 3586 (1993).
[41] B. Bhushan, *Tribology and Mechanics of Magnetic Storage Devices* (Springer, New York, 1990).
[42] T. Miyamoto, R. Kaneko, and S. Miyake, J. Vac. Sci. Technol. B **9**, 1336 (1991).
[43] C. M. Mate, Wear **168**, 17 (1993).
[44] B. Bhushan and B. K. Gupta, J. Appl. Phys. **75**, 6156 (1994).
[45] C. M. Mate, Surf. Coat. Technol. **62**, 373 (1993).
[46] I. Fujiwara, T. Kamei, and K. Tanaka, J. Appl. Phys. **78**, 4189 (1995).
[47] J. Ruan and B. Bhushan, ASME J. Tribol. **116**, 378 (1994).
[48] J. Ruan and B. Bhushan, J. Appl. Phys. **76**, 5022 (1994).
[49] H. W. Kroto, J. R. Heath, S. C. O'Brian, R. F. Curl, and R. E. Smalley, Nature (London) **318**, 162 (1985).
[50] C. S. Yannoni, R. D. Johnson, G. Meijer, D. S. Bethune, and J. R. Salem, J. Phys. Chem. **95**, 9 (1991).
[51] P. J. Blau and C. E. Haberlin, Thin Solid Films **219**, 129 (1992).
[52] B. Bhushan, B. K. Gupta, G. W. Van Cleef, C. Capp, and J. V. Coe, Appl. Phys. Lett. **62**, 3253 (1993).
[53] J. Ruan and B. Bhushan, J. Mater. Res. **8**, 3019 (1993).
[54] T. Thundat, R. J. Warmack, D. Ding, and R. N. Compton, Appl. Phys. Lett. **63**, 891 (1993).
[55] R. Lüthi, H. Haefke, E. Meyer, L. Howald, H.-P. Lang, G. Gerth, and H.-J. Güntherodt, Z. Phys. B **95**, 1 (1994).
[56] R. Lüthi, E. Meyer, H. Haefke, L. Howald, W. Gutmannsbauer, and H.-J. Güntherodt, Science **266**, 1979 (1994).
[57] U. D. Schwarz, W. Allers, G. Gensterblum, J.-J. Pireaux, and R. Wiesendanger, Phys. Rev. B **52**, 5967 (1995).
[58] Nanosensors, Aidlingen, Germany.
[59] K. I. Schiffmann, Nanotechnology **4**, 163 (1993).
[60] Y. Akama, E. Nishimura, and A. Sakai, J. Vac. Sci. Technol. A **8**, 429 (1990).
[61] U. D. Schwarz, O. Zwörner, P. Köster, and R. Wiesendanger, J. Vac. Sci. Technol. B (to be published).
[62] Nanoscope IIIa, Digital Instruments, Santa Barbara, CA, USA.
[63] M. Binggeli and C. M. Mate, J. Vac. Sci. Technol. B **13**, 1312 (1995).
[64] J. Hu, X.-D. Xiao, D. F. Ogletree, and M. Salmeron, Surf. Sci. **327**, 358 (1995).
[65] E. Meyer, R. Lüthi, L. Howald, M. Bammerlin, M. Guggisberg, H.-J. Güntherodt, L. Scandella, J. Gobrecht, A. Schumacher, and R. Prins, in *The Physics of Sliding Friction* (Ref. 13), pp. 349−367.
[66] M. Braun, Labortechnische Geräte, Garching, Germany.
[67] C. M. Mate, in *Handbook of Micro/Nanotribology*, edited by B. Bhushan (CRC Press, Boca Raton, FL, 1995).